Computer Networks and Communications
https://ojs.wiserpub.com/index.php/CNC

Research Article

Channel Estimation and Signal Detection for Massive MIMO under 5G Communication

Pratibha Rani[1*], Arti M. K.[2], Pradeep Kumar Dimri[1]

[1] Department of Electronics Engineering, JC Bose University of Science & Technology (YMCA), Faridabad, India
[2] Department of Electronics and Communication, Netaji Subhas University of Technology, New Delhi, India
E-mail: pratibhaymca@gmail.com

Received: 28 July 2024; **Revised:** 25 October 2024; **Accepted:** 31 October 2024

Abstract: In this article, the space-time transmit technique (STTT) is examined in a massive MIMO environment with Rayleigh fading. The article characterizes the instantaneous signal-to-noise ratio (SNR) for statistical analysis after channel estimation. Singular value decomposition (SVD) is used to get SNR. It provides a closed-form expression for the moment-generating function (MGF) and uses the incomplete moment-generating function (IMGF) to construct the moment's closed-form expression. Key concepts in the fundamentals of communication theory, such as the probability density function (PDF) and cumulative distribution function (CDF), are explored. PDF and CDF plots are obtained for a range of degrees of freedom. Simulation results show that as the degree of freedom increases, a properly normalized sum of the channel information tends toward a normal distribution in STTT which follows central limit theorem.

Keywords: channel estimation, incomplete moment generating function, massive MIMO, performance analysis, probability density function, symbol error rate, cumulative distribution function

Nomenclature

Term	Description
AWGN	Additive white gaussian noise
BS	Base Station
CDF	Cumulative distribution function
CSI	Channel state information
FDD	Frequency division duplexing
MGF	Moment generating function
MIMO	Multiple-input multiple-output
MPSK	M-ary phase-shift key
MLD	Maximum likelihood decoding
PDF	Probability density function
SER	symbol error rate

DOI: https://doi.org/10.37256/cnc.2220245390

STTT	Space-time transmit technique
SVD	Singular value decomposition
TDD	Time division duplexing
2D-GA	Two- dimensional genetic algorithm
GA	genetic algorithm
SINR	Signal to inference noise ratio
TS	Tabu search algorithm
O-RAN	Open radio access network
$\boldsymbol{D}$	Received data matrix
$\boldsymbol{H}$	Channel matrix
$\boldsymbol{T}$	Data transmit matrix
$\boldsymbol{A}$	Additive White Gaussian Noise
q	Transmit antenna
p	Time slots
β	Length of the pilot
k_t	No of antenna at user equipment during uplink
N_r	No of antenna at BS during uplink
$\boldsymbol{\phi}$	Pilot symbol vector
$\boldsymbol{\tau}$	Data symbol vector
$\boldsymbol{\eta}$	Nulling matrix
$\mathbf{W}$	Noise whitening matrix
σ^2	Variance
E(.)	Expectation
$\mathbf{I}$	Identity matrix
$\tilde{.}$	Symbol for estimated value
$\boldsymbol{N_o}$	Noise power
$\boldsymbol{S_o}$	Signal Power
Δ	Signal to noise ratio
$M_\Delta(t)$	Moment generating function
$p(y)$	Probability distribution function for discrete random variable
$f(y)$	Probability distribution function for continuous random variable
$\mathbf{B}$	Diagonal matrix
$\mathbf{F, Q}$	Unitary matrix
$\Gamma(z)$	Gamma function
ε	No. of users
C	Modulation specific function

Note: All the matrix and vectors are represented in bold letters.

1. Introduction

In recent years, wireless technologies have gained significant popularity due to their performance, speed, and coverage, as evidenced by papers [1, 2, 3, 4]. The widespread adoption of tablets, laptops, and smartphones has contributed to the increasing number of consumers. Multiple-input multiple-output (MIMO) communication, as explained in paper [5] was developed to enhance system spectrum efficiency, effectively increasing throughput and supporting a large number of concurrent users. Moreover, massive MIMO is an innovative technique that extends consumer coverage, playing a crucial role in the development of fifth-generation (5G) networks [6, 7, 8, 9, 10]. Massive MIMO involves large number of antennas for transmitting and receiving signals. It is also known as "very large MIMO" and "Full-Dimension MIMO" [11]. Additional antennas, enhance throughput by focusing energy on the user. Other benefits of massive MIMO include reduced

latency, utilization of low-power components, high data rate, high spectral efficiency and broad coverage area. While massive MIMO offers a wide range of advantages, it also has several drawbacks that hinder its use with a large number of antennas. These issues include coherent signal processing, low-cost hardware, hardware flaws, channel characterization, pilot contamination, and channel estimation.

The channel serves as the pathway for transferring data from the transmitter (Tx) to the receiver (Rx). In research papers the majority of studies focus on channel estimation [12, 13, 14, 15, 16, 17, 18, 19]. Some deep learning-based channel estimation strategies are also available. The paper [20] discusses the use of deep learning for improving communication reliability and reducing processing complexity in 5G and 6G networks, but it does not address the inherent complexity and computational demands of deep learning models, which can be a significant barrier for practical implementation in real-world scenarios [21, 22, 23]. The paper [24] provides an in-depth analysis of the intricate nature of beamspace channel estimation algorithms. Despite their reduction in comparison to traditional methods, they continue to pose substantial challenges in practical implementation, primarily due to the requisite employment of advanced mathematical models and significant computational resources [24]. The paper [25] provides a comprehensive analysis of various channel estimation techniques used in millimeter-wave MIMO systems. These techniques are crucial for accurately estimating the channel state information, which is essential for effective communication and data transmission.

Inter-cell interference, referred to as pilot contamination, limits communication in massive MIMO systems [26, 27, 28, 29]. Various pilot assignment schemes have been categorized, including time-shift pilots, fractional frequency reuse, and superimposed pilots [30]. In a time-shifted pilot scheme, each cell is divided into separate groups, one of which simultaneously provides downlink data and uplink pilots. Optimal power allocation is utilized to reduce inter-channel interference for improved communication. The reuse factor for pilots in fractional frequency reuse helps in reducing pilot contamination, as per the research in paper [31, 32]. In superimposed pilots, data and pilots are transmitted through a channel in different time slots while using the TDD mode [32]. In TDD, the same frequency spectrum is utilized for transmission during different time slots for both uplink and downlink. Conversely, frequency division multiplexing (FDD) makes use of dedicated frequency channels for uplink and downlink. The papers [33] introduces a novel pilot assignment scheme that combines a two-dimensional genetic algorithm (2D-GA) with a Tabu-Search algorithm (TS). This integrated approach aims to effectively address the pilot contamination problem. Integrating the 2D-GA with the Tabu-Search algorithm may add complexity to implementation, posing challenges for deployment in real-world systems with limited computational resources. There is another paper [34] that deal with genetic algorithm (GA) and TS. The integration of the genetic algorithm with the Tabu-Search algorithm in paper can lead to increased computational complexity. This may result in longer processing times, particularly in scenarios with a large number of users or channels, potentially hindering real-time applications. Additionally, the numerical simulations presented may assume ideal conditions that do not fully reflect real-world scenarios. There are certain pilot assignment schemes also available for cell-free MIMO [35, 36, 37]. Utilizing multi-agent deep reinforcement learning, the study [38] unequivocally advocates for a decentralized pilot assignment approach to enhance the scalability of open radio access network (O-RAN) cell-free massive MIMO systems while also improving computational scalability and channel prediction performance.

The paper [39] uses a differential phase shift keying (DPSK) method as the basic constellation for single user and multiuser scenarios, this work presents a unique transceiver design that integrates spatial modulation into a non-coherent massive MIMO system. The key differences between coherent and non-coherent are given in the paper [40]:

Channel State Information (CSI):

- **Coherent Detection**: Requires prior knowledge of the channel state information (CSI) at the receiver. This means that the receiver must estimate the channel conditions before detecting the transmitted signal. This process often involves complex channel estimation techniques to accurately capture the fading and noise characteristics of the channel.
- **Non-Coherent Detection**: Does not require explicit channel estimation. Instead, it relies on techniques such as differential encoding, where the information is encoded in the difference between consecutive symbols. This

approach simplifies the detection process, especially in scenarios where channel conditions are rapidly changing or difficult to estimate.

Performance in Different Scenarios:

- **Coherent Detection**: Often provides better performance in stable channel conditions where accurate CSI can be obtained. It is suitable for applications requiring high data rates and reliability, such as in MIMO systems [40].
- **Non-Coherent Detection**: More effective in high-mobility scenarios or environments with significant channel variations, where the overhead of estimating the channel may outweigh the benefits. It is particularly useful for low-complexity applications and can be beneficial in scenarios with high Doppler shifts.

Pilot Overhead:

- **Coherent Detection**: Typically incurs higher pilot overhead due to the need for continuous channel estimation, which can consume valuable spectral resources and power.
- **Non-Coherent Detection**: Reduces pilot overhead, making it more efficient in terms of resource utilization, especially in applications where quick response times are essential.

Complexity:

- **Coherent Detection**: Generally, more complex due to the need for channel estimation and the associated algorithms. This complexity can lead to increased processing requirements and power consumption, particularly in high-mobility environments where channel conditions fluctuate rapidly.
- **Non-Coherent Detection**: Typically, less complex, as it avoids the need for channel estimation. This makes it particularly advantageous for applications like broadcasting and paging, where low latency and reduced overhead are critical.

The authors in the paper [41] propose a novel M-ary Differential Phase Shift Keying (M-DPSK) scheme combined with Bit-Interleaved Coded Modulation and Iterative Decoding (BICM-ID) to reduce the number of antennas needed for effective performance, particularly in time-varying channels. However, the proposed paper deals with coherent detection. The channel state information (CSI) is obtained at the base station (BS) in time-division duplexing (TDD) and BS is capable enough to handle complexity. The proposed paper provides a comfortable space-time transmission technique (STTT) in terms of mathematical computation to get channel information and signal detection. The STTT is pilot assignment scheme which provides a pattern of allocation of pilot and data sequences for channel estimation. The paper approaches coherent detection because of the above-mentioned benefits of coherent communication. Moreover, the presented paper provided deep analysis of moment generating function (MGF), probability density function (PDF) and cumulative distribution function (CDF). CSI is obtained using orthogonal pilot sequences, also known as training symbols or pilots which are necessary to acquire the channel gain.

The presented paper effectively addresses channel estimation in a massive MIMO communication system using orthogonal pilots under the STTT. Notably, we have precisely calculated PDF formulation for various degrees of freedom which is twice the number of receiving antenna. Furthermore, we have successfully derived a CDF. Moreover, the MGF and moment expression are developed. Additionally, we have derived a closed-form expression for the symbol error rate (SER) using M-ary phase-shift key (MPSK) which has been effectively used to analyse the system's performance. Our results unequivocally demonstrate that as the degrees of freedom increases, the system consistently follows the central limit theorem [42], and the PDF reliably approaches a normal distribution, while the SER consistently decreases with the utilization of modulation schemes and the number of antennas.

2. Massive MIMO

The massive MIMO communication system model is shown in Figure 1. This model shows the transmission of signal and channel estimation under uplink from mobile unit to the base station under TDD. The tall, pillar-like structure is the base station or Rx, and the numerous tiny holes on it are the antennas $N_1, N_2, N_3,\ldots, N_r$. The nomenclature for the mobile entities at Tx is a box-like structure with the letters $k_1, k_2, k_3,\ldots, k_t$. Under the TDD technique, transmission takes place between Tx and Rx through wireless communication channel $h_{11}, h_{12}, h_{13}, \ldots, h_{N_r k_t}$. All of the channels are represented collectively in the matrix, H, and are complex Gaussian with unit variance and zero mean. Uplink scenario is used to get the CSI at BS under TDD mode of communication. The schematic diagram of TDD approach is shown in Figure 2. Time Division Duplexing in proposed scheme. The full frequency spectrum can be used by uplink and downlink using TDD. Time is divided into slots, some of which are set aside for uplink and others for downlink. Asymmetric traffic and time-varying uplink and downlink demands are made possible by this method. Additionally, on the premise of channel reciprocity, channel state data computed in the uplink may be utilised in the downlink and there will be no need of downlink pilots. Coherence time is the duration of time under which channel remains constant. The signal and channel estimation is done for coherence time. Similarly, coherence bandwidth is the bandwidth for which channel remains constant. When using a wireless channel for communication, the AWGN accumulates onto the data signal. The noise, A, is supposed to have a zero mean and a variance of σ^2. System model for massive MIMO during uplink is employed with STTT in Figure 1.

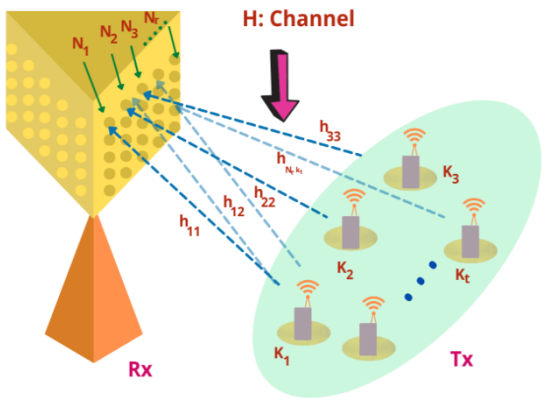

Figure 1. System model for massive MIMO during uplink

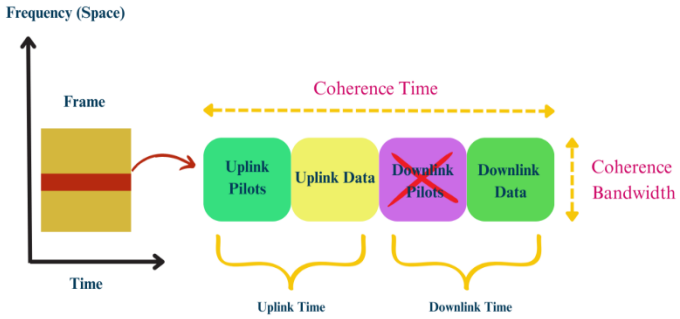

Figure 2. Time division duplexing in proposed scheme

2.1 *Working of proposed scheme*

In order to achieve massive MIMO, STTT is utilised together with an enormous amount of Tx and Rx antennas, as shown in Figure 3.

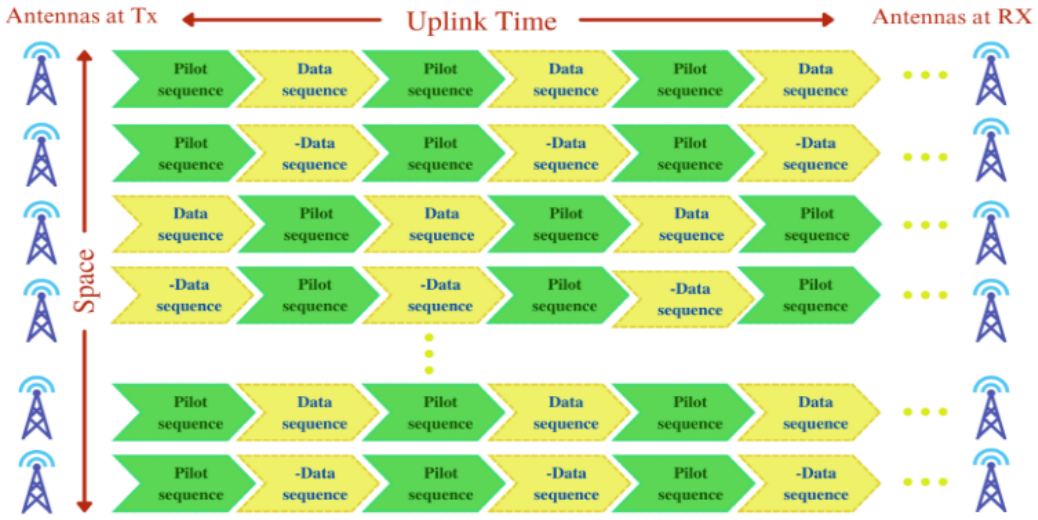

Figure 3. Space-time transmission technique for massive MIMO

In the proposed study, we are focusing on uplink communication for mathematical modeling. We assert that the length of the pilot and data vectors are directly proportional to each other. To implement the scheme, it is essential to have a minimum of four antennas at both the transmitter and receiver. For the sake of simplifying the mathematical simulation, we assert that the number of transmitting and receiving antennas should be rounded up to four in the manuscript. As a result, a 4×4 data transmit matrix called $\boldsymbol{T} \in \mathbb{C}^{4\times4}$ is sent together with a pilot vector. Where the transmit matrix element $\boldsymbol{T_{pq}}$ for $K_t = 4$ and $N_r = 4$ has the values $p \in \{1,2,3,4\}$ and $q \in \{1,2,3,4\}$ respectively. The pilot vector in $\boldsymbol{T}$ is denoted as $\emptyset_{ij}(s)$, $i \in \{1,2,3,4\}$ and is orthogonal to other pilots, meaning that the multiplication of one pilot with another pilot vector is null and $\left|\emptyset_{ij}\right| = 1$. The M-PSK constellation is used to obtain the data vectors.

$$\boldsymbol{T} = \begin{bmatrix} \boldsymbol{T_{11}} & \boldsymbol{T_{12}} & \boldsymbol{T_{13}} & \boldsymbol{T_{14}} \\ \boldsymbol{T_{21}} & \boldsymbol{T_{22}} & \boldsymbol{T_{23}} & \boldsymbol{T_{24}} \\ \boldsymbol{T_{31}} & \boldsymbol{T_{32}} & \boldsymbol{T_{33}} & \boldsymbol{T_{34}} \\ \boldsymbol{T_{41}} & \boldsymbol{T_{42}} & \boldsymbol{T_{43}} & \boldsymbol{T_{44}} \end{bmatrix} = \begin{bmatrix} \boldsymbol{\emptyset_{11}} & \boldsymbol{\tau_{12}} & \boldsymbol{\emptyset_{13}} & \boldsymbol{\tau_{14}} \\ \boldsymbol{\emptyset_{21}} & \boldsymbol{-\tau_{22}} & \boldsymbol{\emptyset_{23}} & \boldsymbol{-\tau_{24}} \\ \boldsymbol{\tau_{31}} & \boldsymbol{\emptyset_{32}} & \boldsymbol{\tau_{33}} & \boldsymbol{\emptyset_{34}} \\ \boldsymbol{-\tau_{41}} & \boldsymbol{\emptyset_{42}} & \boldsymbol{-\tau_{43}} & \boldsymbol{\emptyset_{44}} \end{bmatrix} \quad (1)$$

The transmit matrix elements are described in Equation (1). The pilot's minimum length should match the data vector's length, as shown in Figure 3. In Equation (1) the transmit matrix is represented by the following elements: T_{mn}, where 'm' denotes spatial transmission (transmitting antennas), and 'n' denotes time-domain transmission of a signal. Therefore, it may be stated explicitly that $\boldsymbol{T_{11}}(\boldsymbol{s})$, represent pilot vector transmission through first antennas in first time slot from transmitter (Tx). The data vector transmission through the first antenna in the second time slot from Tx is given as $\boldsymbol{T_{12}}(\boldsymbol{s})$ and other values can be predicted accordingly from the Figure 3. Theoretically, it might be claimed that rows illustrate how communication occurs in time domain, while columns illustrate how it occurs in frequency or space domain.

2.2 *Channel model for STTT*

For the first time slot, the channel model for pilot-based STTT is shown in Figure 4. Four channels, namely h_{11}, h_{21}, h_{31} and h_{41} are mentioned as being utilised for broadcasting the pilot and data vector by the transmitting antenna. Each channel is a complex Gaussian with a zero mean and a unit variance. The signal travels across the channel and is picked up by the receiver, which is the base station during uplink. The received signal is distorted by the noise, $\boldsymbol{A}$, as it travels through the channel. Unwanted signals should be rejected by the receiver. The signal received by the receiver is shown as,

$$\boldsymbol{D} = \boldsymbol{HT} + \boldsymbol{A} \tag{2}$$

The channel matrix for a massive MIMO system is $\boldsymbol{H} \in \mathbb{C}^{N_r \times K_t}$, where $\boldsymbol{A}$ is an AWGN with a variance of σ^2 and zero mean. Practically, the channel is unknown, but getting the channel's information is necessary for trustworthy communication. Pilot or training symbols are used to achieve channel information gain.

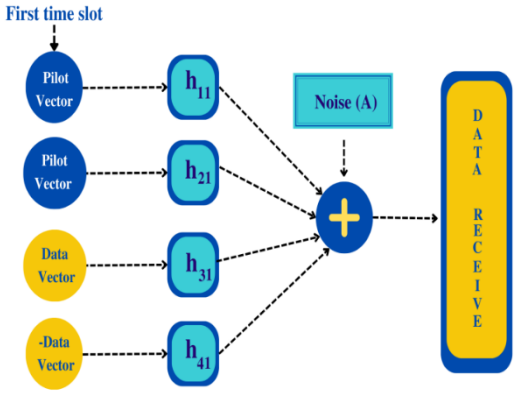

Figure 4. Channel model for first time slot under STTT

The elaborated mathematical expression of the Equation (2) is as follows,

$$\begin{bmatrix} \boldsymbol{D_1} & \boldsymbol{D_2} & \boldsymbol{D_3} & \dots & \boldsymbol{D_\varepsilon} \end{bmatrix} = \begin{bmatrix} \boldsymbol{h_1} & \boldsymbol{h_2} & \boldsymbol{h_3} & \dots & \boldsymbol{h_\varepsilon} \end{bmatrix} \times \begin{bmatrix} \boldsymbol{\phi_{11}} & \boldsymbol{\tau_{12}} & \boldsymbol{\phi_{13}} & \boldsymbol{\tau_{14}} & \cdots & \boldsymbol{\tau_{1j}} \\ \boldsymbol{\phi_{21}} & \boldsymbol{-\tau_{22}} & \boldsymbol{\phi_{23}} & \boldsymbol{-\tau_{24}} & \cdots & \boldsymbol{\tau_{2j}} \\ \boldsymbol{\tau_{31}} & \boldsymbol{\phi_{32}} & \boldsymbol{\tau_{33}} & \boldsymbol{\phi_{34}} & & \boldsymbol{\phi_{3j}} \\ \boldsymbol{-\tau_{41}} & \boldsymbol{\phi_{42}} & \boldsymbol{\tau_{43}} & \boldsymbol{\phi_{44}} & \dots & \boldsymbol{\phi_{4j}} \\ & \vdots & & & \vdots & \\ \boldsymbol{-\tau_{i1}} & \boldsymbol{\phi_{i2}} & \boldsymbol{-\tau_{i3}} & \boldsymbol{\phi_{i4}} & & \boldsymbol{\phi_{ij}} \end{bmatrix} + \begin{bmatrix} \boldsymbol{A_1} & \boldsymbol{A_2} & \dots & \boldsymbol{A_\varepsilon} \end{bmatrix} \tag{3}$$

where, $\boldsymbol{D_\varepsilon} \in \mathbb{C}^{\beta \times p}$, $\boldsymbol{h_\varepsilon} = \begin{bmatrix} h_{1q} & h_{2q} & h_{3q} & \cdots & h_{pq} \end{bmatrix}^T \in \mathbb{C}^{N_r \times 1}$ in which $\boldsymbol{h_\varepsilon}$ represents channel matrix of column vectors, ε indicates number of users, q denotes transmitting antennas and p represents number of time slot to send the signal. It is assumed that the channel won't change while the data is being processed. Transpose is given by $(.)^T$, while the length of the pilot vector is indicated by β. With a variable number of antennas, the received data signal matrix, channel matrix, and noise matrix can be written as,

$$\boldsymbol{D} = \begin{bmatrix} \boldsymbol{D_1} & \boldsymbol{D_2} & \boldsymbol{D_3} & \cdots & \boldsymbol{D_\varepsilon} \end{bmatrix} \in \mathbb{C}^{\{N_r \times (N_r \times N_r)\}}, \tag{4}$$

$$H = \begin{bmatrix} h_1 & h_2 & h_3 & \cdots & h_\varepsilon \end{bmatrix} \in \mathbb{C}^{\{N_r \times K_t\}} \tag{5}$$

and

$$A = \begin{bmatrix} A_1 & A_2 & A_3 & \cdots & A_\theta \end{bmatrix} \in \mathbb{C}^{\{N_r \times (N_r \times N_r)\}} \Big\} \tag{6}$$

For simplicity, considering $K_t = 4$ and $N_r = 4$ in Equation (3) which gives,

$$D_1 = h_1\phi_{11} + h_2\tau_{12} + h_3\phi_{13} + h_4\tau_{14} + A_1 \tag{7}$$

$$D_2 = h_1\phi_{21} - h_2\tau_{22} + h_3\phi_{23} - h_4\tau_{24} + A_2 \tag{8}$$

$$D_3 = h_1\tau_{31} + h_2\phi_{32} + h_3\tau_{33} + h_4\phi_{34} + A_3 \tag{9}$$

$$D_4 = -h_1\tau_{41} + h_2\phi_{42} - h_3\tau_{43} + h_4\tau_{44} + A_4 \tag{10}$$

Gaining access to channel information is an essential aspect of wireless communication for accurate signal detection. The use of the provided equations enables an accurate approximation, and notably, the broadcast pilot vector remains consistent in open spaces. Hence $\phi_{11} = \phi_{21}$ and $\phi_{13} = \phi_{23}$. Here it is assumed that the data from first and second user in only second time slot and fourth time slots are equal. Finally, the result of adding Equations (7) and (8) is,

$$\frac{D_1 + D_2}{2} = h_1\phi_{11} + h_3\phi_{13} + \frac{A_1 + A_2}{2} \tag{11}$$

The orthogonal pilots are known at the receiving end [10]. As a result, Equation (11) is multiplied by the hermitian $(.)^H$ of ϕ_{11} . Therefore, $\phi_{11}^H\phi_{13} = 0$ and $\phi_{11}\phi_{11}^H = 1$ using the orthogonal property of the pilots.

$$\left[\frac{D_1 + D_2}{2}\right]\phi_{11}^H = \underbrace{h_1}_{Original channel} + \underbrace{\left[\frac{A_1 + A_2}{2}\right]\phi_{11}^H}_{Noise} \tag{12}$$

where estimated channel becomes,

$$\widetilde{h_1} = h_1 + \underbrace{\left[\frac{A_1 + A_2}{2}\right]\phi_{11}^H}_{Noise}, \tag{13}$$

Equations (7) and (8) can also be used to estimate $\widetilde{h_3}$ and Equations (9) and (10) can be used to determine other channel information. Finally, CSI look like,

$$\tilde{H} = \begin{bmatrix} \widetilde{h_1} & \widetilde{h_2} & \widetilde{h_3} & \widetilde{h_4} \end{bmatrix} \tag{14}$$

where, $\widetilde{\boldsymbol{h_i}}$ is the column channel information from i^{th} transmit antenna to all receiving antennas and $\widetilde{\boldsymbol{H}}$ is the complete estimated channel matrix.

2.3 *Maximum likelihood detection*

In any transmission, the data signal must be received and retrieved at the receiver for it to be considered reliable. The process of distinguishing between informative patterns and random patterns is known as signal detection. Random patterns are generally referred to as noise [43]. Detection theory include application in communications, quality assurance, mobile communication, psychology, etc. This idea, which is also employed in artificial intelligence and confusion matrices, is closely related to signal to noise ratio.

The noise that gathers with the signal entering via the channel must be removed in order to detect the ideal signal. The receiver in the proposed technique uses CSI to detect data. Data information at the receiving end is obtained via the space null property. We can get the following from Equations (7) and (8),

$$\frac{\boldsymbol{D_1}-\boldsymbol{D_2}}{\boldsymbol{2}}=\boldsymbol{h_2\tau_{12}}+\boldsymbol{h_4\tau_{14}}+\frac{\boldsymbol{A_1}-\boldsymbol{A_2}}{\boldsymbol{2}} \tag{15}$$

From Equations (7) and (8), it is assumed that the data from first and second user in only second time slot and fourth time slots are equal $\tau_{12}=\tau_{22}$ and $\tau_{14}=\tau_{24}$. Equation (15) is subjected to space nulling, which entails multiplying it by the nulling matrices [10, 44, 45] as $\boldsymbol{\eta_4}=\left(null\left(\widetilde{h}_4^H\right)\right)^H$ to obtain,

$$\boldsymbol{\eta_4}\left(\frac{\boldsymbol{D_1}-\boldsymbol{D_2}}{\boldsymbol{2}}\right)=\boldsymbol{\eta_4 h_2\tau_{12}}+\underbrace{\boldsymbol{\eta_4 h_2\tau_{12}}}_{\boldsymbol{0}}+\boldsymbol{\eta_4}\frac{\boldsymbol{A_1}-\boldsymbol{A_2}}{\boldsymbol{2}}, \tag{16}$$

Nulling's property states that $\boldsymbol{\eta_4 h_4}=\boldsymbol{0}$. The left null of any column vector with more than two elements is a matrix, as shown by simulation [10, 44]. Equation now becomes,

$$\boldsymbol{\eta_4}\left(\frac{\boldsymbol{D_1}-\boldsymbol{D_2}}{\boldsymbol{2}}\right)=\boldsymbol{\eta_4 h_2\tau_{12}}+\boldsymbol{\eta_4}\,\frac{\boldsymbol{A_1}-\boldsymbol{A_2}}{\boldsymbol{2}}, \tag{17}$$

Noise whitening is done in order to eliminate noise,

$$\boldsymbol{\Lambda}=\boldsymbol{W_1}^{\left(-\frac{1}{2}\right)}\boldsymbol{\eta_4}\left(\frac{\boldsymbol{D_1}-\boldsymbol{D_2}}{\boldsymbol{2}}\right)=\mathbf{W}_1^{\left(-\frac{1}{2}\right)}\boldsymbol{\eta_4 h_2\tau_{12}}+\mathbf{W}_1^{\left(-\frac{1}{2}\right)}\boldsymbol{f_1} \tag{18}$$

In the aforementioned equation, $\boldsymbol{f_1}=\boldsymbol{\eta_4}\left(\frac{\boldsymbol{A_1}-\boldsymbol{A_2}}{\boldsymbol{2}}\right)$. The AWGN matrix has the same parameters that are taken into account for noise, namely zero mean and σ^2 variance. The frequency band being used for effective communication has a uniform power distribution. The term for noise whitening is given as, $W_1=E\left(\boldsymbol{\eta_4}\left(\frac{\boldsymbol{A_1}-\boldsymbol{A_2}}{\boldsymbol{2}}\right)\boldsymbol{\eta_4}\left(\frac{\boldsymbol{A_1}-\boldsymbol{A_2}}{\boldsymbol{2}}\right)\right)$. Here, $E(.)$ represents expectation operator. After simulation it is observed that $\boldsymbol{\eta_4\eta_4^H}=\boldsymbol{I}$ and $\boldsymbol{I}$ is the identity matrix. Therefore, $\boldsymbol{W_1}=\frac{\sigma^2}{2}\boldsymbol{I}$.

Now, $\boldsymbol{\tau_{12}}$ is detected using MLD. The paper contains the initial research on MLD [43, 46, 47]. By maximising the conditional PDF of the δ condition on $\boldsymbol{\eta_4}$ and $\boldsymbol{h_2}$, $\boldsymbol{\tau_{12}}$ is obtained. Therefore, we get,

$$\widehat{\boldsymbol{\tau_{12}}}=\boldsymbol{\arg\min_{\widehat{\tau_{12}}}}||\boldsymbol{\delta_1}-\boldsymbol{W_1}^{-\frac{1}{2}}\boldsymbol{\eta_4 h_2}\widetilde{\boldsymbol{\tau_{12}}}||^2, \tag{19}$$

Likewise we can get other data values as,

$$\widehat{\tau_{14}} = \arg\min_{\widehat{\tau_{14}}} ||\delta_2 - W_2^{-\frac{1}{2}} \eta_4 h_4 \widetilde{\tau_{14}}||^2, \tag{20}$$

$$\widehat{\tau_{22}} = \arg\min_{\widehat{\tau_{22}}} ||\delta_3 - W_3^{-\frac{1}{2}} \eta_4 h_1 \widetilde{\tau_{22}}||^2, \tag{21}$$

$$\widehat{\tau_{24}} = \arg\min_{\widehat{\tau_{12}}} ||\delta_4 - W_4^{-\frac{1}{2}} \eta_4 h_3 \widetilde{\tau_{24}}||^2, \tag{22}$$

where $\delta_1 = \delta_2 = \left(\frac{D_1 - D_2}{2}\right)$, $\delta_3 = \delta_4 = \left(\frac{D_1 - D_4}{2}\right)$, $W_1 = W_2 = W_3 = W_4 = \frac{\sigma^2}{2} I$, $\eta_i = \left(null\left(\widehat{h_i}^H\right)\right)^H$ and i = 1, 2, 3 and 4 are considered case of $N_r = 4$ and $N_t = 4$.

3. Performance evaluation

It is assumed in the above equation that the channel information is available at the receiver. However, this will never actually be the case. Therefore, Equation (14) is used to get the estimated CSI. The following equations are used to develop the signal to noise ratio under estimated CSI,

$$\widehat{\tau_{12}} = \arg\min_{\widehat{\tau_{12}}} \delta_1 - W_1^{\frac{1}{2}} \tilde{\eta}_4 \tilde{h}_2 \widetilde{\tau_{12}}^2, \tag{23}$$

Now, signal power, S_o, and noise power, N_o are,

$$S_o = \frac{2}{\sigma^2} \left\| \eta_4 h_2 \left(\tau_{12} - \widetilde{\tau_{12}}\right) \right\|^2 \tag{24}$$

$$N_o = \|\kappa_1\|^2 - \left\| W_1^{\frac{-1}{2}} \eta_4 q_e \phi_{13}^H \widetilde{\tau_{12}} \right\|^2 \tag{25}$$

In that case, $\kappa_1 = W_1^{-\frac{1}{2}} \eta_4 \left(\frac{A_1 - A_2}{2}\right)$. Evaluation reveals that κ is constant, thus for the sake of simplicity, we have considered it 2. Additionally, noise becomes,

$$N_o = 2 - \left(W_1^{\frac{-1}{2}} \eta_4 q_e \phi_{13}^H \widetilde{\tau_{12}} \right) \left(W_1^{\frac{-1}{2}} \eta_4 q_e \phi_{13}^H \widetilde{\tau_{12}} \right)^H \tag{26}$$

In above equation, $q_e = \left(\frac{A_1 + A_2}{2}\right)$ whereas, $W_1^{-\frac{1}{2}} * W_1^{-\frac{1}{2}^H} = \frac{2}{\sigma^2}$, $\eta_4 * \eta_4^H = I$, $q_e * q_e^H = \sigma^2$ and $\tau_{12} * \widetilde{\tau_{12}} = 1$. Collectively, the noise power is represented as,

$$N_o = 2 - 2||\phi_{13}||^2 \tag{27}$$

Now, Equations (24) and (27) gives SNR i.e., $\Delta = \frac{S_O}{N_O}$ as,

$$\Delta_1 = \frac{\frac{2}{\sigma^2}\left\|\boldsymbol{\eta_4 h_2}\left(\boldsymbol{\tau_{12}} - \widetilde{\boldsymbol{\tau_{12}}}\right)\right\|}{2 - 2\left\|\boldsymbol{\phi_{13}}\right\|^2} \tag{28}$$

$$\Delta_1 = \frac{E\left|\tau_{12} - \widetilde{\tau_{12}}\right|^2 \left\|\boldsymbol{\eta_4 h_2}\right\|^2}{\sigma^2\left(1 - \left\|\boldsymbol{\phi_{13}}\right\|^2\right)} \tag{29}$$

3.1 *Moment generating function and moments*

Moment generating function (MGF) and moments are statistical parameters to evaluate the performance of the system.

3.1.1 *Moment generating function*

MGF for SNR has been evaluated in the paper [48, 49]. MGF of $n \times 1$ random SNR (Δ) is given by,

$$M_\Delta(t) = E\left[e^{t\Delta}\right], \tag{30}$$

where $t = (t_1, t_2, t_3, \ldots, t_n)'$ and expectation exist for $-\boldsymbol{h} < \boldsymbol{t_j} < \boldsymbol{h}$ where $\boldsymbol{h} > \boldsymbol{0}$ and $j = 1, 2, 3 \ldots, n$ and basic MGF expression for continuous and discrete random variable Y is given by [50],

$$M_Y(s) = E\left[e^{sY}\right] = \left\{\int_{-\infty}^{\infty} e^{sy} f(y)\, dy, \qquad if\ Y\ is\ continuos\right. \tag{31}$$

In the above equation $f(y)$ are the probability density function (PDF). Since IMGF of SNR is the laplace transform. Singular value decomposition [10, 44, 45] is employed to obtain SNR in relation to Equation (28),

$$||\boldsymbol{\eta_4 h_2}||^2 = ||\boldsymbol{BFQ^H h_2}||^2 = ||\boldsymbol{BF}\widetilde{\boldsymbol{h_2}}||^2, \tag{32}$$

where $\boldsymbol{B}$ is the diagonal matrix, $\boldsymbol{F}$, and $\boldsymbol{Q}$ are the unitary matrix. Since, $\widetilde{\boldsymbol{h_2}} = \boldsymbol{Q^H h_2}$, $\widetilde{\boldsymbol{h_2}}$ has same distribution as $\boldsymbol{h_2}$ i.e., circularly symmetric complex Gaussian. Further,

$$||\boldsymbol{BF}\widetilde{\boldsymbol{h_2}}||^2 = \widetilde{\boldsymbol{h_2}}^{\boldsymbol{H}} \boldsymbol{F^H B^H BF}; \widetilde{\boldsymbol{h_2}}, \tag{33}$$

where in above equation $\boldsymbol{B^H B = I}$ i.e., Identity matrix. Therefore, equation becomes,

$$||\boldsymbol{BF}\widetilde{\boldsymbol{h_2}}||^2 = \widetilde{\boldsymbol{h_2}}^{\boldsymbol{H}} \boldsymbol{F^H F}\widetilde{\boldsymbol{h_2}} = ||\boldsymbol{F}\widetilde{\boldsymbol{h_2}}||^2 = \boldsymbol{F_1}|\boldsymbol{h_{11}}|^2 + \boldsymbol{F_2}|\boldsymbol{h_{12}}|^2 + \boldsymbol{F_3}|\boldsymbol{h_{13}}|^2 + \ldots = |\boldsymbol{h_{11}}|^2 + |\boldsymbol{h_{12}}|^2 + |\boldsymbol{h_{13}}|^2 + \ldots, \tag{34}$$

This represents that the distribution will be central chi-square with $2N_r$ degree of freedom. The degree of freedom is directly proportional to the number of receiving antennas. Higher degrees of freedom in massive MIMO systems lead to enhance SNR through spatial diversity, good beamforming, multiplexing gains, enhance channel estimation, reduced interference, and the averaging effects of large antenna arrays. This results in enhanced performance and capacity of the communication system [51].

Hence instantaneous SNR in Equation (28) becomes,

$$\Delta_i = \sum_{i=1}^{N_r-1} \left|\widetilde{h_{1i}}\right|^2 * \beta * \widetilde{\Delta_i} \tag{35}$$

where, $\boldsymbol{\beta}$ deals with pilot length. PDF for chi-square distribution for random variable Y is given as [50]

$$P_Y(y) = \frac{1}{2^{\frac{d}{2}}\Gamma\left(\frac{d}{2}\right)} y^{\left(\frac{d}{2}-1\right)} e^{\frac{d}{2\sigma^2}} \quad for y > 0, \tag{36}$$

where $\boldsymbol{d}$ represents degree of freedom. Using Equations (31) and (36) we have IMGF as,

$$M_{\Delta_i}(s) \triangleq \int_0^{\infty} \exp(-s\Delta_i) \frac{\Delta_i^{N_r-1} \exp\left(-\frac{\Delta_i}{2\sigma^2}\right)}{2^{N_r}\Gamma(N_r)} d\Delta_i \tag{37}$$

$$\begin{aligned} M_{\Delta_i}(s) &\triangleq \frac{1}{2^{N_r}\Gamma(N_r)} \int_0^{\infty} \Delta_i^{N_r-1} e^{(-s\Delta_i)} e^{\left(-\frac{\Delta_i}{2\sigma^2}\right)} d\Delta_i, \\ &\triangleq \frac{1}{2^{N_r}\Gamma(N_r)} \int_0^{\infty} \Delta_{\mathrm{i}}^{N_r-1} \mathrm{e}^{-\left(s\Delta_{\mathrm{i}}+\frac{\Delta_{\mathrm{i}}}{2\sigma^2}\right)} d\Delta_{\mathrm{i}}, \phi \end{aligned} \tag{38}$$

Now Let,

$$\frac{1}{2^{N_r}\Gamma(N_r)} = q,$$

$$N_r = a,$$

$$\Delta_i = t$$

$$s\Delta_i + \frac{\Delta_i}{2\sigma^2} = p$$

Above equation can be reduced to,

$$M_{\Delta_i}(s) = q \int_0^{\infty} t^{a-1} e^{-pt} dt \tag{39}$$

The factorial function to nonintegral values is known as the gamma function [52] and it is given as,

$$\Gamma(z) = \int_0^{\infty} t^{z-1} e^{-t} dt \tag{40}$$

After taking into account $z-1 = b$, the equation is changed in accordance with the characteristic of the gamma function as,

$$\int_0^{\infty} t^b e^{-pt} dt = \frac{\Gamma(b+1)}{p^{b+1}} \tag{41}$$

On comparing Equations (39) and (41) we obtain,

$$M_{\Delta_i} = \frac{q}{p^{a-1}} \int_0^{\infty} \Gamma(\Delta_i)\, d\Delta_i \tag{42}$$

On comparing above integral with the equation 3.381.7 in [53]

$$M_{\Delta_i}(s) = \frac{1}{\left(1 + 2s\beta\bar{\Delta}_i\right)^{N_r}} \tag{43}$$

3.1.2 *Moments*

The moments provide the information about the properties of the distribution. The moments of random variable describe the characteristics of random variable [54, 55].

First Moment (Mean): The distribution's mean, or expected value, is the first moment. It provides an indication of the data's central placement and a gauge of its propensity to cluster.

Second Moment (Variance): The variance, which measures the dispersion of the data, is the second moment around the mean. The data are more dispersed from the mean when the variance is bigger.

Third Moment (Skewness): The distribution's asymmetry is explained by the third moment. A long right tail (data concentrated on the left) is indicated by a positive skewness, and a long-left tail is indicated by a negative skewness.

Fourth Moment (Kurtosis): The distribution's tailiness is gauged by the fourth moment. A distribution with a high kurtosis has heavier tails, or more outliers, than one with a low kurtosis.

The moment-generating function in signal processing offers a means of encoding every moment of a random variable. It facilitates the analysis of signal and noise characteristics. In the paper, SNR is the random variable and moments with respect to SNR are required to get the statistical analysis of probability density function.

Successive differentiation of MGF with respect to instantaneous SNR gives moments as [56],

$$M'_{\Delta_i}(s) = \frac{d}{d\Delta_i} E\left[e^{s\Delta_i}\right], = E\left[\frac{d}{d\Delta_i}\left(e^{s\Delta_i}\right)\right] = E\left[se^{s\Delta_i}\right] \tag{44}$$

As a result, the first moment is the mean and it is given by,

$$M'_{\Delta_i}(0) = E[\Delta_i], \tag{45}$$

Likewise,

$$M''_{\Delta_i}(s) = \frac{d}{d\Delta_i} M'_{\Delta_i}(s) = \frac{d}{d\Delta_i} E\left[se^{s\Delta_i}\right] = E\left[\frac{d}{d\Delta_i}\left(se^{s\Delta_i}\right)\right]. \tag{46}$$

After differentiation we get second moment which is a variance,

$$M''_{\Delta_i}(0) = E\left[\Delta_i^2\right], \tag{47}$$

Finally, the n^{th} derivative of $M(s)$ evaluated at $s = 0$ is,

The distribution is determined exclusively by the MGF. Although the expression in Equation (31) corresponds to a complete MGF, in the real world of wireless communication, an incomplete MGF (IMGF), also known as a truncated or interval MGF, is employed [54, 56]. IMGF expression looks like this,

$$M_{\Delta_i}^{n}(0) = E\left[\Delta_i^{n}\right], n \geq 1 \tag{48}$$

With the help of an IMGF derivative, moments of the IMGF are obtained. The first moment (mean) is presented as,

$$\mu_{\Delta_i} = \frac{\partial M_{\Delta_i}(s)}{\partial \Delta_i} = \frac{\partial}{\partial \Delta_i}\left(\frac{1}{\left(1+2s\beta\bar{\Delta}_i\right)^{N_r}}\right) \tag{49}$$

Let,

$$G^{p} = \frac{1}{\left(1+2s\beta\bar{\Delta}_i\right)^{N_r}} \tag{50}$$

where considering $p = N_r$. After comparing Equation (50) with the equation AD (73.7.1),0.434 in [53], we get n^{th} moment as,

$$\frac{\partial^n G^p}{\partial s^n} = p\binom{n-p}{n}\left\{-\binom{n}{1}\frac{1}{p-1}G^{p-1}\frac{\partial^n G}{\partial s^n} + \binom{n}{2}\frac{1}{p-2}G^{p-2}\frac{\partial^n G}{\partial s^n} - \ldots\right\} \tag{51}$$

Therefore the n^{th} moment is given as,

$$\begin{aligned}\frac{\partial^n M_{\Delta_i}(s)}{\partial \Delta_i^{n}} &= (N_r)\binom{n-(N_r)}{n}\left\{-\binom{n}{1}\frac{1}{N_r-1}\left(\frac{1}{(1+2s\beta\bar{\Delta}_i)}\right)^{N_r-1}\frac{\partial^n}{\partial s^n}\left(\frac{1}{(1+2s\beta\bar{\Delta}_i)}\right)\right.\\ &\left.+\binom{n}{2}\frac{1}{N_r-2}\bar{\Delta}_i\left(\frac{1}{(1+2s\beta\bar{\Delta}_i)}\right)^{N_r-2}\frac{\partial^n}{\partial s^n}\left(\frac{1}{(1+2s\beta\bar{\Delta}_i)}\right)^{2} - \ldots\right\}\end{aligned} \tag{52}$$

The value of moments can directly be obtained from above equation by simply putting the value of n. For first second and third moment, it is $n = 1, n = 2$ and $n = 3$.

3.1.3 *Symbol error rate*

One of the important aspects in communication engineering is SER. The likelihood that a transmitted signal would unintentionally be demodulated into one of its closest neighbors in the signal constellation is represented by SER. The relation that is used to obtain SER using the IMGF expression is, symbol used in Equation (53) are noted as, $\vartheta_k = \frac{\pi(M-1)}{M}$ and modulation specific function, $C = \sin^2\left(\frac{\pi}{M}\right)$ where $M = 4$ in case of quadrature phase shift key (QPSK) modulation, $M = 8$ for 8-PSK and $M = 16$ for 16-PSK. Further, equation is developed as [50, 57].

$$\Omega_c = \frac{1}{\pi}\int_0^{\vartheta_k} M_{\Delta_i}\left(\frac{C}{\sin^2\theta}\right)d\theta, \tag{53}$$

$$\Omega_c \approx \sum_{s=1}^{3} \psi_s M_{\Delta_i}(\Lambda_s), \tag{54}$$

where $\boldsymbol{\psi_1 = \frac{\vartheta_k}{2\pi} - \frac{1}{6}}$, $\boldsymbol{\psi_2 = \frac{1}{4}}$, $\boldsymbol{\psi_3 = \frac{\vartheta_k}{2\pi} - \frac{1}{4}}$, $\boldsymbol{\Lambda_1 = \vartheta_k}$, $\boldsymbol{\Lambda_2 = \left(\frac{4\vartheta_k}{3}\right)}$ and $\boldsymbol{\Lambda_3 = \frac{\vartheta_k}{\sin^2\theta_M}}$. Now, close form expression of SER is obtained as,

$$\Omega_c \approx \sum_{s=1}^{3} \frac{\psi_s}{(1+\psi_s \beta \Delta_i)^{N_r}}. \tag{55}$$

3.1.4 *Expression for probability density function and cumulative distribution function*

$E\left[Q\left(\sqrt{\Delta_i}\right)\right]$ returns the average bit error [52, 58, 59] where $Q(.)$ is the Gaussian-Q function. For the purpose of analyzing the inaccuracy in digital communication, Q-Function is a crucial parameter. $Q(\Delta_i)$ is the likelihood that the normal random variable will have an amount greater than Δ_i. Typically, the expression for the Q-Function is as follows:

$$Q(\Delta_i) = \frac{1}{\sqrt{2\pi}} \int_{\Delta_i}^{\infty} e\left(\frac{\Delta_i^2}{2}\right) d\Delta_i \tag{56}$$

Therefore,

$$Q(\Delta_i) = 1 - Q(-\Delta_i) = 1 - \Theta(\Delta_i), \tag{57}$$

where $Q(\Delta_i)$ is the CDF of the standard normal Gaussian distribution and $\Theta(\Delta_i)$d in terms of error function it is given as [50]

$$\Theta(\Delta_i) = \frac{1}{2} erfc\left(\frac{\Delta_i}{\sqrt{2}}\right). \tag{58}$$

PDF of Chi- square distributed variable is given in Equation (42) and according to the definition of CDF,

$$F_\Delta(\Delta_i) = P(\Delta \le \Delta_i) = 1 - P_\Delta(\Delta_i) = \int_{-\infty}^{\Delta_i} P(\Delta_i)\, d\Delta_i \tag{59}$$

$$F_\Delta(\Delta_i) = \int_{-\infty}^{y} \frac{1}{2^{\frac{d}{2}}\Gamma\left(\frac{d}{2}\right)} \Delta_i^{\left(\frac{d}{2}-1\right)} e^{\frac{d}{2\sigma^2}}\, d\Delta_i \tag{60}$$

In terms of degree of freedom, it is represented as,

$$F_\Delta(\Delta_i; d) = \frac{\gamma\left(\frac{d}{2}, \frac{\Delta_i}{2}\right)}{\Gamma\left(\frac{d}{2}\right)} = P\left(\frac{d}{2}, \frac{\Delta_i}{2}\right), \tag{61}$$

where $\gamma(.,.)$ is the lower incomplete gamma function *and* $P(.,.)$ is the regularized gamma function.

4. Result

Equation (55) is used to depict the fluctuation of SER with system configuration and modulation strategy. The system configuration and data presented in the Table 1 are simulated using MATLAB software. In the table $\boldsymbol{\phi}$ represents the number of pilots used with variable length, $\boldsymbol{\tau}$ indicates the data random values, $\boldsymbol{H}$ is the channel matrix with Gaussian normal distribution with zero mean and unit variance, $\boldsymbol{A}$ is the additive white Gaussian noise with zero mean and $\boldsymbol{\sigma^2}$ variance. MPSK modulation scheme is used with M = 4, 8 and 16. Total number of samples considered in the simulation is 1000 and variable SNR is used in simulation part.

Table 1. Experimental parameters used during simulation in MATLAB.

Parameters	Values
$\boldsymbol{\phi_{11}}$	[1 0 0 0], [1 0 0 0 0 0 0 0], [1 0 0 0 0 0 0 0 0 0 0 0 0 0 0 0], ...
$\boldsymbol{\phi_{13}}$	[0 1 0 0], [0 1 0 0 0 0 0 0], [0 1 0 0 0 0 0 0 0 0 0 0 0 0 0 0], ...
$\boldsymbol{\phi_{21}}$	[0 0 1 0], [0 0 1 0 0 0 0 0], [0 0 1 0 0 0 0 0 0 0 0 0 0 0 0 0], ...
$\boldsymbol{\phi_{23}}$	[0 0 0 1], [0 0 0 1 0 0 0 0], [0 0 0 1 0 0 0 0 0 0 0 0 0 0 0 0], ...
$\tau_{12},\ \tau_{14}\ ,\ \tau_{22},\ \tau_{24}$	Random values
$\boldsymbol{H}$	$\mathcal{N}(0,1)$
$\boldsymbol{A}$	$\mathcal{N}(0,\sigma^2)$
Modulation Scheme	QPSK, 8-PSK, 16- PSK
Samples	1000
Degree of freedom (d)	$2N_r$
N_t	4, 8
N_r	4, 8, 16, 32, 36, 40, 42
SNR	−10 to 20

SER plot is obtained for downlink time to get receive diversity. The SER plot in Figure 5 shows that the minimum SER for QPSK, 8-PSK and 16-PSK at SNR = 3 dB is 0.026, 0.047 and 0.136 respectively. On comparison 8-PSK and 16-PSK, SER for QPSK under 4×4 system is minimum. That is why QPSK is the best for digital transmission as compare to 8-PSK and 16-PSK.

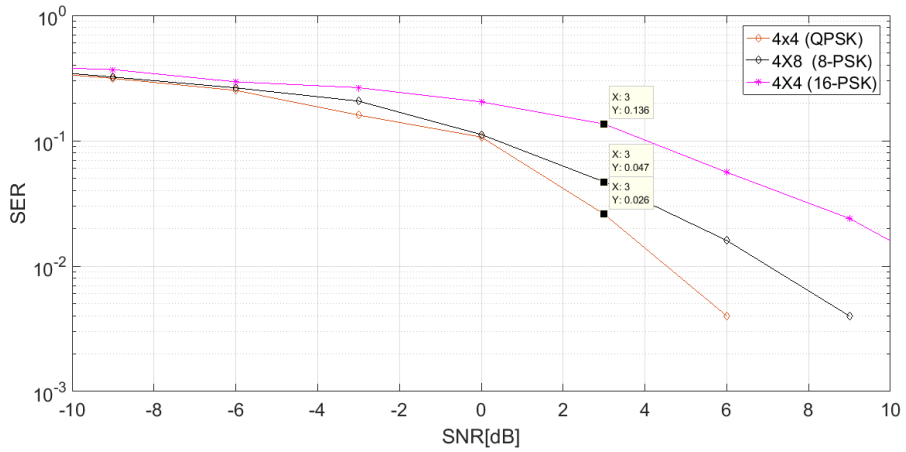

Figure 5. SER comparison under different modulation schemes and system configuration

Figure 6 is the analytical plot for QPSK modulation with varying number of transmitting and receiving antenna. The values of SER for SNR = 6 is 0.002768, 0.001246, $3.43e^{-5}$, $4.761e^{-7}$, $1.55e^{-8}$, $9.845e^{-16}$ for 4×4, 8×8, 8×16, 8×32, 8×36, 8×42 under QPSK modulation. This can be concluded from the plot that as the number of antennas increses the SER decreases.

Figure 7 shows the probability density function of the SER with respect to SNR for varying number of receiving antenna. It is observed that as the number of receiving antennas increases the plot follows the gaussian distribution and the probability of SER decreases as number of antennas increases. Additionally, As the degree of freedom rises, the PDF plot proves the central limit theorem and produces a Gaussian distribution The central limit theorem states that the sampling distribution of the mean will always be approximately normally distributed, provided the sample size is sufficiently large.

The Figure 8 in the massive MIMO communication system shows the CDF for varying number of transmitting and receiving antennas using Equation (61). For 4×4, 4×8, 4×32, 4×40 the CDF reaches to saturation at SNR = 17, 15, 13 and 11 respectively. The graphic demonstrates that CDF hits saturation at lower SNR as degree of freedom grows. It means the occurrence of the signal detection surpassing this point is highly improbable, with the probability being almost negligible.

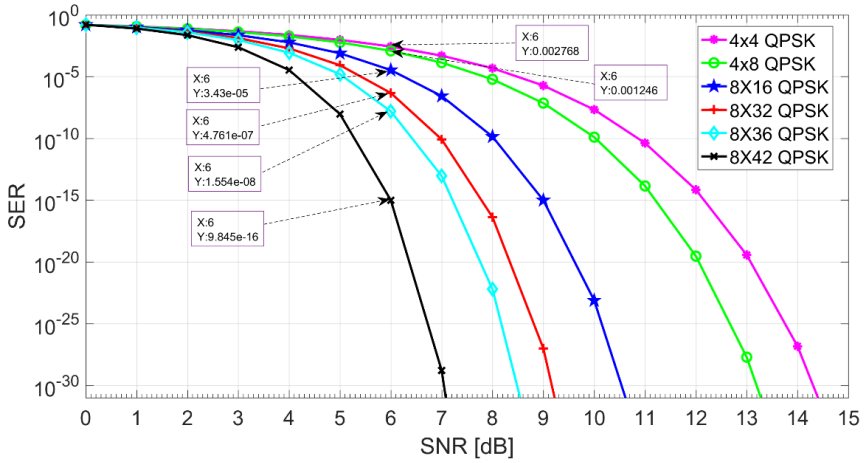

Figure 6. SER for varying number of antennas under QPSK modulation for STTT

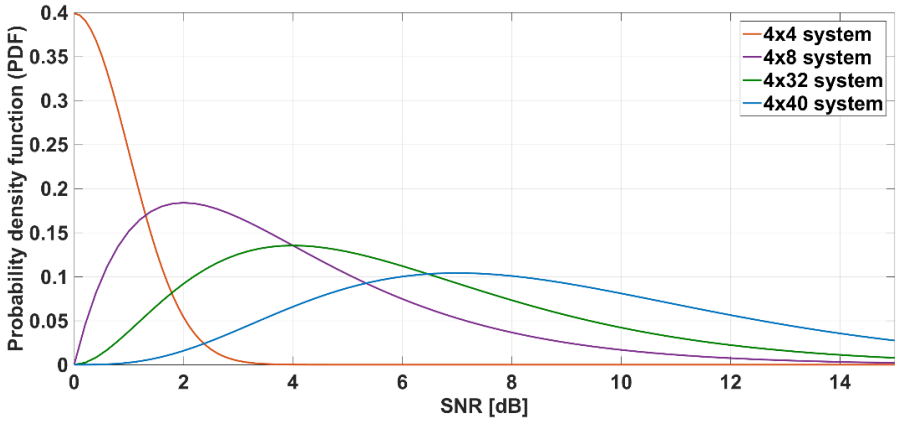

Figure 7. PDF for varying system configuration i.e., 4 × 4, 4 × 8, 4 × 32 and 4 × 40

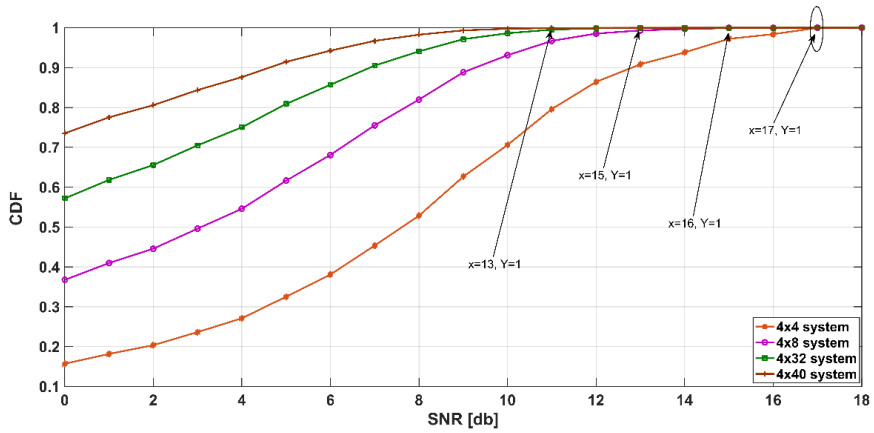

Figure 8. CDF for varying system configuration i.e., 4 × 4, 4 × 8, 4 × 32 and 4 × 40

5. Conclusions

In a massive MIMO system architecture, channel gain estimation is achieved using STTT under TDD. This approach capitalizes on the use of orthogonal pilot sequences. The IMGF is effectively utilized to calculate SER with QPSK demonstrating superior performance compared to other modulation schemes in a massive MIMO scenario. We have rigorously derived closed-form expressions for the IMGF, PDF, CDF and moments. Notably, as the degrees of freedom increase, the PDF plot consistently demonstrates a Gaussian distribution, aligning with the central limit theorem. At lower SNR levels, the CDF attains saturation with increasing degrees of freedom. STTT emerges as an effective method for massive MIMO systems housing numerous receiving antennas. Furthermore, it is worthwhile to explore additional research avenues involving orthogonal frequency-division multiplexing (OFDM).

Conflict of interest

There is no conflict of interest for this study.

References

[1] E. Bjornson, J. Hoydis, and L. Sanguinetti, "Massive MIMO Has Unlimited Capacity," *IEEE Trans. Wirel. Commun.*, vol. 17, no. 1, pp. 574–590, 2018.

[2] E. G. Larsson, O. Edfors, F. Tufvesson, and T. L. Marzetta, "Massive MIMO for Next Generation Wireless Systems," *IEEE Commun. Mag.*, vol. 52, no. 2, pp. 186–195, 2014.

[3] I. Elmutasim, "A Brief Review of Massive MIMO Technology for the Next Generation," *Int. Arab J. Inf. Technol.*, vol. 20, no. 2, 2023, https://doi.org/10.34028/iajit/20/2/13.

[4] T. L. Marzetta, E. G. Larsson, H. Yang, and H. Q. Ngo, *Fundamentals of Massive MIMO*, Cambridge, UK: Cambridge University Press, 2016, https://doi.org/10.1017/CBO9781316799895.

[5] S. Yang and L. Hanzo, "Fifty Years of MIMO Detection: The Road to Large-Scale MIMOs," *IEEE Commun. Surv. Tutorials*, vol. 17, no. 4, 2015, https://doi.org/10.1109/COMST.2015.2475242.

[6] O. Elijah, C. Y. Leow, T. A. Rahman, S. Nunoo, and S. Z. Iliya, "A Comprehensive Survey of Pilot Contamination in Massive MIMO-5G System," *IEEE Commun. Surv. Tutorials*, vol. 18, no. 2, 2016, https://doi.org/10.1109/COMST.2015.2504379.

[7] M. Ke, Z. Gao, Y. Wu, X. Gao, and K.-K. Wong, "Massive Access in Cell-Free Massive MIMO-Based Internet of Things: Cloud Computing and Edge Computing Paradigms," *IEEE J. Sel. Areas Commun.*, vol. 39, no. 3, pp. 756–772, Mar. 2021, https://doi.org/10.1109/JSAC.2020.3018807.

[8] L. Lu, G. Y. Li, A. L. Swindlehurst, A. Ashikhmin, and R. Zhang, "An Overview of Massive MIMO: Benefits and Challenges," *IEEE J. Sel. Topics Signal Process.*, vol. 8, no. 5, pp. 742–758, 2014.

[9] H. N. Qureshi, M. Manalastas, S. M. A. Zaidi, A. Imran, and M. O. Al Kalaa, "Service Level Agreements for 5G and Beyond: Overview, Challenges and Enablers of 5G-Healthcare Systems," *IEEE Access*, vol. 9, pp. 1044–1061, 2021, https://doi.org/10.1109/ACCESS.2020.3046927.

[10] P. Rani, M. K. Arti, P. K. Dimri, and M. Vashishath, "Pilot Based Space-Time Transmission Scheme for Large MIMO System," in *Proc. 2019 6th Int. Conf. Signal Process. Integr. Netw., SPIN 2019*, Noida, India, Mar. 7–8, 2019.

[11] K. Zheng, S. Ou, and X. Yin, "Massive MIMO Channel Models: A Survey," *Int. J. Antennas Propag.*, vol. 2014, no. 1, p. 848071, 2014, https://doi.org/10.1155/2014/848071.

[12] F. A. Pereira De Figueiredo, D. A. Mendes Lemes, C. Ferreira Dias, and G. Fraidenraich, "Massive MIMO Channel Estimation Considering Pilot Contamination and Spatially Correlated Channels," *Electron. Lett.*, vol. 56, no. 8, 2020, https://doi.org/10.1049/el.2019.3899.

[13] H. Xie, F. Gao, S. Jin, J. Fang, and Y. C. Liang, "Channel Estimation for TDD/FDD Massive MIMO Systems with Channel Covariance Computing," *IEEE Trans. Wirel. Commun.*, vol. 17, no. 6, pp. 4206–4218, 2018, https://doi.org/10.1109/TWC.2018.2821667.

[14] J. Yuan, H. Q. Ngo, and M. Matthaiou, "Machine Learning-Based Channel Estimation in Massive MIMO with Channel Aging," in *Proc. IEEE Wkshp. Signal Process. Adv. Wireless Commun., SPAWC*, Cannes, France, Jul. 2–5, 2019. https://doi.org/10.1109/SPAWC.2019.8815557.

[15] K. Mei, J. Liu, X. Zhang, N. Rajatheva, and J. Wei, "Performance Analysis on Machine Learning-Based Channel Estimation," *IEEE Trans. Commun.*, vol. 69, no. 8, pp. 5183–5193, Aug. 2021, https://doi.org/10.1109/TCOMM.2021.3083597.

[16] P. Sure and C. M. Bhuma, "A Survey on OFDM Channel Estimation Techniques Based on Denoising Strategies," *Eng. Sci. Technol. Int. J.*, vol. 20, no. 2, 2017, https://doi.org/10.1016/j.jestch.2016.09.011.

[17] W. Yang, M. Li, and Q. Liu, "A Practical Channel Estimation Strategy for XL-MIMO Communication Systems," *IEEE Commun. Lett.*, vol. 27, no. 6, 2023, https://doi.org/10.1109/LCOMM.2023.3266821.

[18] B. Hassan, S. Baig, H. M. Asif, S. Mumtaz, and S. Muhaidat, "A Survey of FDD-Based Channel Estimation Schemes with Coordinated Multipoint," *IEEE Syst. J.*, vol. 16, no. 3, 2022, https://doi.org/10.1109/JSYST.2021.3111284.

[19] R. Zhang, L. Yang, M. Tang, W. Tan, and J. Zhao, "Channel Estimation for mmWave Massive MIMO Systems With Mixed-ADC Architecture," *IEEE Open J. Commun. Soc.*, vol. 4, p. 3242668, 2023, https://doi.org/10.1109/OJCOMS.2023.3242668.

[20] M. Susandhika and A. Shirly Edward, "A Comprehensive Review and Comparative Analysis of 5G and 6G Based MIMO Channel Estimation Techniques," in *ICRTEC 2023—Proc. IEEE Int. Conf. Recent Trends Electron. Commun.: Upcoming Technol. Smart Syst.*, Mysore, India, Feb. 10–11, 2023.

[21] Z. Yuan, J. Zhang, Y. Ji, G. F. Pedersen, and W. Fan, "Spatial Non-Stationary Near-Field Channel Modeling and Validation for Massive MIMO Systems," *IEEE Trans. Antennas Propag.*, vol. 71, no. 1, 2023, https://doi.org/10.1109/TAP.2022.3218759.

[22] Y. Chen, M. Mancini, X. Zhu, and Z. Akata, "Semi-Supervised and Unsupervised Deep Visual Learning: A Survey," *IEEE Trans. Pattern Anal. Mach. Intell.*, vol. 46, no. 3, pp. 1327–1347, Mar. 2024, https://doi.org/10.1109/TPAMI.2022.3201576.

[23] R. Suresh, H. Bishnoi, A. V. Kuklin, A. Parikh, M. Molokeev, R. Harinarayanan, et al., "Revolutionizing physics: a comprehensive survey of machine learning applications," *Front. Phys.*, vol. 12, p. 1322162, 2024, https://doi.org/10.3389/fphy.2024.1322162.

[24] S. G. Daware, P. Engineer, and S. N. Shah, "A review on Beamspace Channel Estimation Algorithms in Wireless Communication," in *Proc. 2023 IEEE 7th Conf. Inf. Commun. Technol., CICT 2023*, Jabalpur, India, Dec. 15–17, 2023, https://doi.org/10.1109/CICT59886.2023.10455367.

[25] C. V. V. S. Srinivas and S. Borugadda, "A Comprehensive Review on Channel Estimation Methods for Millimeter Wave MIMO Systems," in *Lecture Notes of the Institute for Computer Sciences, Social-Informatics and Telecommunications Engineering, LNICST*. Cham, Switzerland: Springer Nature, 2023, https://doi.org/10.1007/978-3-031-28975-0_21.

[26] Y. Zhang, X. Qiao, L. Yang, and H. Zhu, "Superimposed Pilots are Beneficial for Mitigating Pilot Contamination in Cell-Free Massive MIMO," *IEEE Wireless Commun. Lett.*, vol. 25, no. 1, pp. 279–283, 2021, https://doi.org/10.1109/LCOMM.2020.3024705.

[27] Y. Wu, T. Liu, M. Cao, L. Li, and W. Xu, "Pilot contamination reduction in massive MIMO systems based on pilot scheduling," *EURASIP J. Wirel. Commun. Netw.*, vol. 2018, Mar. 2018, https://doi.org/10.1186/s13638-018-1029-1.

[28] S. Stein Ioushua and Y. C. Eldar, "Pilot Sequence Design for Mitigating Pilot Contamination With Reduced RF Chains," *IEEE Trans. Commun.*, vol. 68, no. 6, pp. 3536–3549, Jun. 2020, https://doi.org/10.1109/TCOMM.2020.2979142.

[29] T. L. Marzetta, J. Jose, A. Ashikhmin, and S. Vishwanath, "Pilot Contamination and Precoding in Multi-Cell TDD Systems," *IEEE Trans. Wirel. Commun.*, vol. 10, no. 8, pp. 2640–2651, 2014.

[30] A. Misso, M. Kissaka, and B. Maiseli, "Exploring pilot assignment methods for pilot contamination mitigation in massive MIMO systems," *Cogent Eng.*, vol. 7, no. 1, 2020, https://doi.org/10.1080/23311916.2020.1831126.

[31] L. Su and C. Yang, "Fractional Frequency Reuse Aided Pilot Decontamination for Massive MIMO Systems," in *Proc. 2015 IEEE 81st Veh. Technol. Conf. (VTC Spring)*, Glasgow, UK, May 11–14, 2015, pp. 1–6, https://doi.org/10.1109/VTCSpring.2015.7145845.

[32] K. Upadhya, S. A. Vorobyov, and M. Vehkapera, "Superimposed Pilots Are Superior for Mitigating Pilot Contamination in Massive MIMO," *IEEE Trans. Signal Process.*, vol. 65, no. 11, pp. 2917–2932, Jun. 2017, https://doi.org/10.1109/TSP.2017.2675859.

[33] H. T. Gidena and K. S. Weldemichael, "A new pilot assignment scheme for mitigating pilot contamination in uplink massive multi-input – multi-output (MIMO) systems," *EURASIP J. Wirel. Commun. Netw.*, vol. 2024, no. 1, 2024, https://doi.org/10.1186/s13638-023-02329-1.

[34] A. Misso and M. Kissaka, "Pilot contamination mitigation by pilot assignment and adaptive linear precoding for massive MIMO multi-cell systems," *Telecommun. Syst.*, vol. 85, no. 3, 2024, https://doi.org/10.1007/s11235-023-01093-3.

[35] L. Zhang, S. Yang, and Z. Han, "Pilot Assignment for Cell-Free Massive MIMO: A Spectral Clustering Approach," *IEEE Wireless Commun. Lett.*, vol. 13, no. 1, 2024, https://doi.org/10.1109/LWC.2023.3327079.

[36] Y. Chen, X. Zhang, F. Yao, K. An, G. Zheng, and S. Chatzinotas, "Pilot Assignment and Power Control in Secure UAV-Enabled Cell-Free Massive MIMO Networks," *IEEE Internet Things J.*, vol. 11, no. 2, 2024, https://doi.org/10.1109/JIOT.2023.3296736.

[37] T. H. Nguyen, L. T. Phan, and T. Van Chien, "An efficient location-based pilot assignment in Cell-Free Massive MIMO," *ICT Express*, vol. 9, no. 5, 2023, https://doi.org/10.1016/j.icte.2022.09.005.

[38] M. S. Oh, A. B. Das, S. Hosseinalipour, T. Kim, D. J. Love, and C. G. Brinton, "A Decentralized Pilot Assignment Algorithm for Scalable O-RAN Cell-Free Massive MIMO," *IEEE J. Sel. Areas Commun.*, vol. 42, no. 2, 2024, https://doi.org/10.1109/JSAC.2023.3336154.

[39] V. M. Baeza, "Incorporating Spatial Modulation for Non-Coherent Massive MIMO With DPSK Schemes," *IEEE Wireless Commun. Lett.*, vol. 13, pp. 2527–2530, 2024, https://doi.org/10.1109/LWC.2024.3424286.

[40] C. Xu, N. Ishikawa, R. Rajashekar, S. Sugiura, R. G. Maunder, Z. Wang, et al., "Sixty Years of Coherent Versus Non-Coherent Tradeoffs and the Road from 5G to Wireless Futures," *IEEE Access*, vol. 7, pp. 178246–178299, 2019, https://doi.org/10.1109/ACCESS.2019.2957706.

[41] V. M. Baeza, A. Garcia Armada, M. El-Hajjar, and L. Hanzo, "Performance of a Non-Coherent Massive SIMO M-DPSK System," in *Proc. 2017 IEEE 86th Vehicular Technol. Conf. (VTC Fall): Proc.*, Toronto, Canada, Sept. 24–27, 2017. https://doi.org/10.1109/VTCFall.2017.8288015.

[42] J. Hu, W. Li, and W. Zhou, "Central Limit Theorem for Mutual Information of Large MIMO Systems with Elliptically Correlated Channels," *IEEE Trans. Inf. Theory*, vol. 65, no. 11, 2019, https://doi.org/10.1109/TIT.2019.2913760.

[43] J. I. Marcum, "A Statistical Theory of Target Detection By Pulsed Radar," *IRE Trans. Inf. Theory*, vol. 6, no. 2, pp. 59–267, 1960, https://doi.org/10.1109/TIT.1960.1057560.

[44] P. Rani, M. K. Arti, and P. K. Dimri, "Capacity for Space Time Data Transmission Scheme in Colocated Massive MIMO," in *Proc. 3rd Int. Conf. Smart Electron. Commun., ICOSEC 2022—Proceedings*, Trichy, India, Oct. 20–22, 2022, pp. 120–126, https://doi.org/10.1109/ICOSEC54921.2022.9951993.

[45] M. K. Arti, "OSTBC Transmission in Large MIMO Systems," *IEEE Commun. Lett.*, vol. 20, no. 11, pp. 2308–2311, Nov. 2016, https://doi.org/10.1109/LCOMM.2016.2597229.

[46] F. Y. Edgeworth, "On the Probable Errors of Frequency-Constants (Contd.)," *J. Royal Stat. Soc.*, vol. 71, no. 3, pp. 499–512, Sep. 1908, https://doi.org/10.1111/j.2397-2335.1908.tb02703.x.

[47] X. Zhu and R. D. Murch, "Performance Analysis of Maximum Likelihood Detection in a MIMO Antenna System," *IEEE Trans. Commun.* vol. 50, no. 2, pp. 187–191, 2002.

[48] G. Chu, K. Niu, W. Wu, and F. Yang, "MGF-Based Analysis of Spectrum Sensing over K-μ Fading Channels for 5G Cognitive Networks," *IEEE Access*, vol. 6, pp. 78650–78658, 2018, https://doi.org/10.1109/ACCESS.2018.2885132.

[49] N. Kim and H. Park, "Bit Error Performance of Convolutional Coded MIMO System with Linear MMSE Receiver," *IEEE Trans. Wirel. Commun.*, vol. 8, no. 7, pp. 3420–3424, Jul. 2009, https://doi.org/10.1109/TWC.2009.080938.

[50] J. G. Proakis and M. Salehi, *Digital Communications*, 5th ed. New York, NY, USA: McGraw Hill, 2007.

[51] A. Liu, L. Lian, V. K. N. Lau, and X. Yuan, "Downlink Channel Estimation in Multiuser Massive MIMO with Hidden Markovian Sparsity," *IEEE Trans. Signal Process.*, vol. 66, no. 18, pp. 4796–4810, Sep. 2018, https://doi.org/10.1109/TSP.2018.2862420.

[52] S. Atapattu, C. Tellambura, and H. Jiang, "A Mixture Gamma Distribution to Model the SNR of Wireless Channels," *IEEE Trans. Wirel. Commun.*, vol. 10, no. 12, 2011, https://doi.org/10.1109/TWC.2011.111210.102115.

[53] I. S. Gradshteyn, I. M. Ryzhik, *Table of Integrals, Series, and Products*, 7th ed. Boston, MA, USA: Academic press, 2007.

[54] S. M. Ross, "Chapter 4—Random Variables and Expectation," in *Introduction to Probability and Statistics for Engineers and Scientists (Sixth Edition)*, S. M. Ross, Ed. New York, NY, USA: Academic Press, 2021, pp. 99–150, https://doi.org/10.1016/B978-0-12-824346-6.00013-2.

[55] X. Wang, "Moment Generating Function of Uncertain Variable," in *Proc. 2018 10th Int. Conf. Intell. Human-Machine Syst. Cybern., IHMSC 2018*, Hangzhou, China, Aug. 25–26, 2018, vol. 1, pp. 129–132.

[56] F. J. Lopez-Martinez, J. M. Romero-Jerez, and J. F. Paris, "On the Calculation of the Incomplete MGF With Applications to Wireless Communications," *IEEE Trans. Commun.*, vol. 65, no. 1, pp. 458–469, Jan. 2017, https://doi.org/10.1109/TCOMM.2016.2626440.

[57] M. K. Arti and M. R. Bhatnagar, "Maximal Ratio Transmission in AF MIMO Relay Systems over Nakagami-m Fading Channels," *IEEE Trans. Veh. Technol.*, vol. 64, no. 5, pp. 1895–1903, May 2015, https://doi.org/10.1109/TVT.2014.2334631.

[58] A. Behnad, "A Novel Extension to Craig's Q-Function Formula and Its Application in Dual-Branch EGC Performance Analysis," *IEEE Trans. Commun.*, vol. 68, no. 7, 2020, https://doi.org/10.1109/TCOMM.2020.2986209.

[59] G. K. Karagiannidis and A. S. Lioumpas, "An Improved Approximation for the Gaussian Q-Function," *IEEE Commun. Lett.*, vol. 11, no. 8, 2007, https://doi.org/10.1109/LCOMM.2007.070470.